Pages: 127-144 / Vol. 18 / Issue 2 / Summer-Fall 2025

Journal of Aerospace Science and Technology

Journal Homepage: https://jast.ias.ir

Original Research Article

Evaluation of Non-Turbopump Feed Systems for Application in a Two-Stage Launch Vehicle

Mehran Nosratollahi[1]*, Hanieh Es-haghnia[2], and Amirhossien Adami[3]

1, 2, 3. Faculty of Aerospace, Malek Ashtar University of Technology, Tehran, Iran

ARTICLE INFO

Received: 09 October 2024
Revised: 17 January 2025
Accepted: 21 January 2025
Available online: 30 September 2025

KEYWORDS:

Launcher
Propulsion system
Pressure-fed system feeding
Multidisciplinary design optimization

DOI: https://doi.org/10.22034/jast.2025.482120.1211

ABSTRACT

Given the significant cost associated with space missions, optimizing launch vehicles (LVs) has been a major focus. The main component of a launch vehicle, and a significant contributor to its cost, is the propulsion system. Propulsion systems can be primarily categorized into two types based on their feeding mechanisms: pump-fed and pressure-fed.. This paper considers the development of non-turbopump propulsion systems for optimum LV design. To this purpose, the disciplines of modeling LV have been presented. Multidisciplinary design optimization of non-turbopump LV is proposed based on the All At Once framework, and validation has been given. The desired mission is to send the maximum payload mass into a 250 km orbit with the minimum total mass of the LV. According to the results, the new optimal Gas Pressure Fed LV concept is introduced as a low-cost and efficient launcher in terms of mass, dimensions, and performance. By mission optimization, the optimal GPF-LV can carry and inject 1857 kg of payload with 85.602 tons of gross mass (μ_pay=0.02169) into a 250 km orbit.

Nomenclature

A	Nozzle cross-sectional area	P_t	Nozzle throat pressure
a_t	Nozzle throat sound speed	P_{tank}	Propellant tank pressure
B	Blowdown ratio	P_{tankf}	The pressure of the fuel tank
D_{LV}	Launch vehicle diameter	P_{tankox}	The pressure of the oxidizing tank
D_{stage}	Stage diameter	R	Gas constant
g	Gravity acceleration	R_t	Radius of the throat nozzle
H_{orb}	Altitude of the destination orbit	T_c	Combustion chamber temperature
H_{LV}	Orbital altitude of the launch vehicle	T_t	Nozzle throat temperature
L^*	Characteristic length of the combustion chamber	t_{burn}	Burning time
L_c	Chamber length	V_{gi}	Initial ullage volume
L_n	Nozzle length	V_{gf}	Final ullage volume
L_{LV}	Launch vehicle length	V_{gtf}	Pressurant tank volume for fuel
L_{stage}	Stage length	V_{gtox}	Pressurant tank volume for oxidizer
M_i	Mach	V_{LV}	Orbital velocity of the launch vehicle
M_e	Mach of the combustion products at the nozzle exit	V_{orb}	Velocity of destination orbit

M_{prop}	The total mass of the propellant
M_{pay}	Payload mass
M_{LV}	The gross mass of the launch vehicle
$\dot{m}_{eng}$	The mass flow rate of the engine
m_{fuel}	Fuel mass
m_{ox}	Oxidizer mass
m_{gox}	Mass of pressurant gas for oxidizer
m_{gfuel}	Mass of pressurant gas for fuel
N_{eng}	Number of engines
N_{fin}	Number of fins
n	Load factor
OF	Mixture ratio
P_{gi}	Initial gas pressure
P_{gf}	Final gas pressure
T_{tank}	Tank temperature
V_{tf}	Fuel tank volume
V_{tox}	Oxidizer tank volume
V_u	Consumption propellant volume
W_u	Consumption propellant weight
Φ	Latitude of the launch site
ε	Nozzle surface expansion ratio
γ	Specific heat ratio
ϵ_c	Chamber surface contraction ratio
θ_c	Chamber narrowing angle
θ_{nose}	Fairing nose angle
ρ_{str}	Structural density
Subscripts	
t	Nozzle throat
e	Nozzle exit
c	Combustion chamber

1 INTRODUCTION

Given the space industry's cost constraints, particularly the high cost of development [1, 2], simplified yet robust approaches are highly desirable [3]. A primary objective of any new space mission is to reduce transportation costs [4-7]. Because launch vehicle (LV) costs constitute a significant portion of overall mission expenses, optimal LV design is crucial. The propulsion subsystem, a major cost driver, is, therefore, a key focus of optimization efforts. Multidisciplinary Design Optimization (MDO) offers an effective approach by simultaneously addressing interacting design aspects applicable to systems such as space transportation [8, 9] and propulsion [10, 11]. Recently, pressurized propulsion systems have garnered renewed interest as an alternative to turbopump systems due to their higher reliability and lower development costs. A propulsion system comprises key components, including the thruster, feeding subsystem, propellant tanks, and control systems. The feeding subsystem's function is to deliver liquid propellant to the combustion chamber at the required flow rate and pressure. Based on feeding type, propulsion systems are classified into two main types, including pump-fed and pressure-fed. To evaluate two types, the following can be mentioned [12]:

Pump-fed propulsion, typically used for high-thrust applications, maximizes performance (thrust and specific impulse) and allows for lighter tanks. However, these systems are more complex, expensive, less reliable, and require more complex handling procedures, especially for cryogenic propellants. Pressure-fed systems are suitable for lower-thrust and prioritize simplicity, reliability, lower cost, and ease of operation. This comes at the cost of reduced performance and potentially heavier tanks. While pump-fed systems offer greater performance potential, the advantages of pressure-fed systems in terms of reliability and cost make them suitable for specific applications.

Pressure-fed propulsion systems have a long history in rocketry, offering a simpler and often more reliable alternative to pump-fed systems, particularly for specific applications. These applications in launch vehicles include Early Rockets (the German V-2), Sounding Rockets (for atmospheric research and suborbital experiments), Upper Stages (orbital insertion and payload delivery), and Small Launch Vehicles (the first stage of SpaceX's Falcon 1). A review of the literature reveals several key developments. A novel self-pressurizing fuel tank without a high-pressure gas vessel is proposed in [13], suitable for micro-thrusters. Other uses of the pressurization system can be found for small bipropellant rocket engines in Refs. [14-17,9]; the Morpheus lunar lander in Ref. [18], and upper/second stages in Refs. [19, 20]. Hybrid rocket engines have also been proposed as applications of this type of feeding system [21, 22]. Reference [23], discusses the development and optimization of a tridyne pressurization system for pressure-fed launch vehicles. A modular optimization framework for designing optimal liquid propellant pressure-fed rocket engines for launch vehicles is developed in. [24]. Since researchers and designers have recently focused on the utilization of pressure-fed propulsion systems in complex space vehicles, with the exception of the system described in [23], these launch vehicles were not designed to use pressure-fed systems in all stages. In addition, LVs such as Scorpius and the second stage of Falcon-1 (as mentioned above) have used Jet-A and RP-1 as fuel, respectively, which presents opportunities for potential improvements.

1.1 Feeding systems

Pressure-feeding systems themselves fall into two types: self-pressurized and gas-pressurized. All types of fed systems are illustrated in Fig. 1.

While pressure-fed systems have found applications in the upper stages, the feasibility of a fully pressure-fed launch vehicle (LV) remains an open question due to their lower performance and higher mass requirements. This paper addresses this gap by evaluating LV designs based exclusively on pressure-fed propulsion. The advantages and disadvantages of these systems are summarized in Table 1.

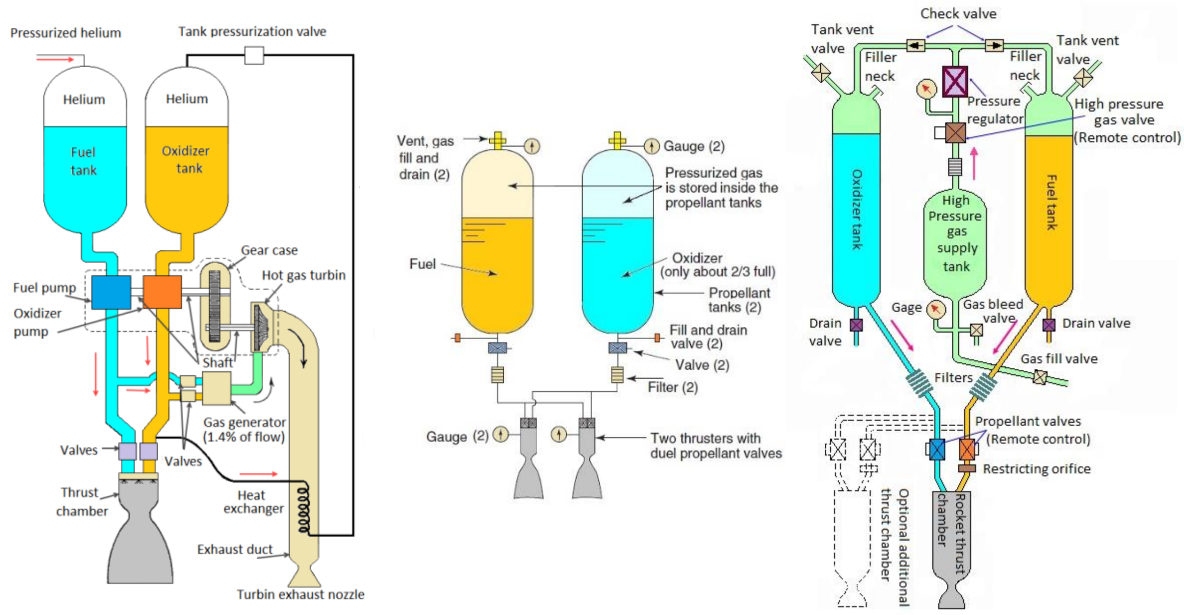

(a) (b) (c)

Fig 1. Feeding systems (a) Turbopump, (b) Self-Pressure Fed (SPF), (c) Gas-Pressure Fed (GPF) [25]

Table 1. Comparison of two types of pressure-fed systems.

Feeding type	Gas-pressurization	Self-pressurization
Advantages	Much constant thrust Feed propulsion at constant pressure and mass flow rate Better control of the mixing ratio Ullage volume is 10-30% of the pressurant tank	The simplest way of feeding/High-reliability Cheaper and with fewer components Less pressurant gas is required Do not use a separate pressurant tank
Disadvantages	Relatively more complex The greater the amount of pressurant gas required Use separate tanks for pressurant gas	Ullage volume is 30-60% of the propellant tanks Reduce thrust and I_{sp} by consuming propellants Storage of propellants at high-pressure The engine must be stable over a wide range of thrust values and mixing ratios.

While a subsystem-level analysis suggests the use of GPF, a system-level perspective, particularly in a complex system like an LV, may yield different conclusions. Therefore, due to incomplete knowledge of each type's overall effectiveness and potential, both GPF-LV and SPF-LV designs should be explored.

This research considers methane as a fuel due to its lower volumetric density and non-toxic nature. Methane's non-toxicity reduces environmental impact mitigation requirements, consequently lowering costs. The benefits of using methane as a propellant include:

- Easier and cheaper access compared to other conventional propellants.
- Non-toxic, non-corrosive, self-draining, and easy to purge.
- Reduced environmental impact mitigation requirements.
- Higher density than liquid hydrogen (six times denser), allowing for greater mass storage in a smaller volume.
- Thermal compatibility with liquid oxygen (both cryogenic at approximately 90 K and 111 K, respectively) enables the use of common components for fuel and oxidizer, thus reducing costs.
- Lowest heat capacity among hydrocarbon fuels, making it suitable for regenerative cooling.

This study proposes reducing the number of LV stages to two, compared to the three stages used in the pressure-fed Scorpius LV, as another cost-reduction measure. Finally, a multidisciplinary design optimization algorithm for a pressure-fed LV is presented to explore potentially novel and optimal solutions.

2 PROBLEM DEFINITION

The purpose of this research is to develop a new approach to designing a liquid launch vehicle by changing the propulsion system from a turbopump to pressure-fed. Using a pressurized feeding propulsion system leads to simplicity, lower development cost and risk, shorter development time, high reliability, fewer components, lower tolerance, easy and quick startup/ shut down, and higher robustness of handling [21-23]. For any optimal design, a clear definition of the mission is essential.

2.1. Mission Description

Traditional launch vehicle (LV) mission definitions specify a fixed payload mass to be delivered to a fixed orbit. However, this approach presents challenges for this research due to potential limitations in available technology, such as specific impulse I_{sp} and thrust level, which may preclude delivering arbitrary payloads to any desired orbit. Therefore, a simultaneous optimization of both the mission and LV design was adopted. Specifically, the payload mass ratio ($\mu_{pay} = \frac{M_{pay}}{M_{LV}}$) was selected as a system variable, with the goal of maximizing payload mass delivered to orbital altitude while minimizing total LV mass. Design parameters, limitations, and assumptions include the use of composite tanks (for reduced weight and dimensions) and green propellants (methane/oxygen).

2.2. Assumptions

The following design assumptions were made: (a) identical diameters for the first and second stages and (b) a fixed thrust level for the thruster used in both stages. As previously mentioned, two LV configurations were designed: one based on an SPF system and the other on a GPF system.

3 DISCIPLINES MODELING AND RELATIONSHIPS

Multidisciplinary Design Optimization (MDO) is a set of engineering system design methods that effectively manage interactions between multiple disciplines. The purpose of MDO methods is to leverage these interdisciplinary couplings between different disciplines to achieve an overall optimized design. MDO is the main focus of development in space systems design processes that manage several disciplines simultaneously. This optimization can be performed at a discipline level or system level. As shown in Fig. 2, MDO problems can be single-objective or multi-objective and can be solved using various architectures, including single-level (e.g., AAO, MDF, IDF) or multi-level methods (e.g., CO, CSSO, BLISS).

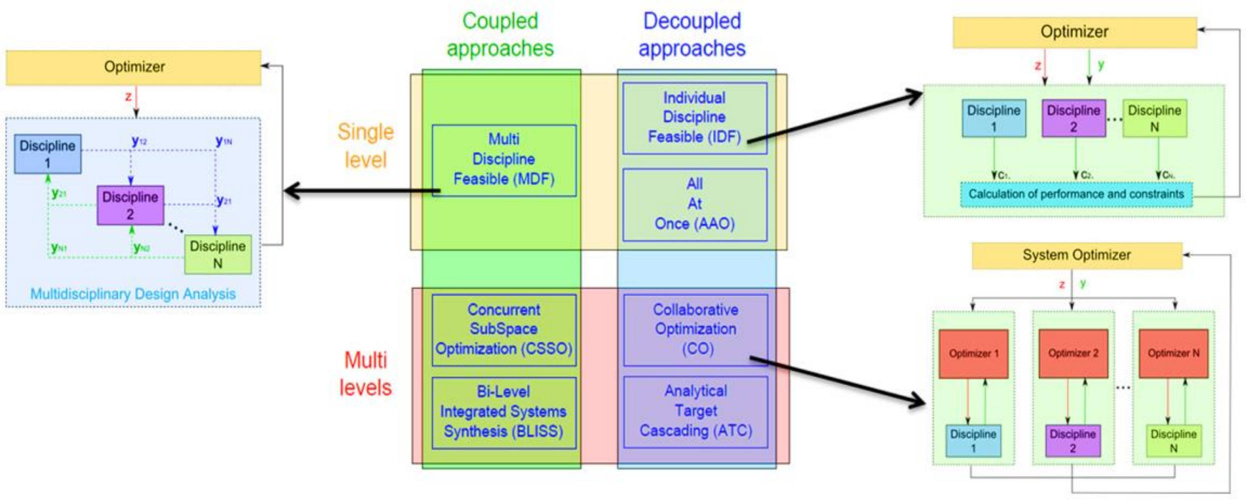

Fig 2. Classic formulation of MDO [23].

The following disciplines are considered for optimal LV design: (1) Propulsion, (2) Feeding System, (3) Structure, (4) Aerodynamics, and (5) Trajectory and Pitch Program. The modeling of these disciplines is presented below.

3.1. Propulsion discipline

The propulsion discipline encompasses the engine and propellant tanks.

3.1.1. Engine

The engine comprises the combustion chamber, nozzle, cooling system, injector, and cap. As shown in Fig. 3, thrust and specific impulse are calculated using Equations (1) and (2), respectively:

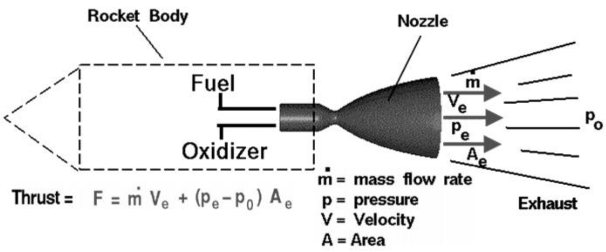

Fig 3. Thrust equation [26]

$$T_{vac} = \frac{A^* P_e(\gamma M_e^2+1)}{M_e^2}\left[\frac{2}{\gamma+1}\left(1+\frac{\gamma-1}{2}M_e^2\right)\right]^{\frac{\gamma+1}{2(\gamma-1)}} \quad (1)$$

$$Isp_{vac} = \frac{T_{vac}}{\dot{m}g_0} \quad (2)$$

Because the process within the thrust chamber is assumed to be an isentropic process (constant entropy), thermodynamic relationships can be used to determine pressure, temperature, sound speed, and density at various points within the chamber, given the specific heat ratio and other properties of the desired gas. These relationships are expressed in Equations (3) through (6) [26-28]:

$$\frac{\rho_t}{\rho} = \left[1+\frac{\gamma-1}{2}M^2\right]^{\frac{1}{\gamma-1}} \quad (3)$$

$$\frac{a_t}{a} = \left[1+\frac{\gamma-1}{2}M^2\right]^{0.5} \quad (4)$$

$$\frac{P_t}{P} = \left[1+\frac{\gamma-1}{2}M^2\right]^{\frac{\gamma}{\gamma-1}} \quad (5)$$

$$\frac{T_t}{T} = \left[1+\frac{\gamma-1}{2}M^2\right]^{\frac{1}{\gamma-1}} \quad (6)$$

The relationship between the nozzle area ratio and the Much number is given in equation (7) [27, 29]:

$$\frac{A}{A^*} = \frac{1}{M}\left[\frac{2}{\gamma+1}\left(1+\frac{\gamma-1}{2}M^2\right)\right]^{\frac{\gamma+1}{2(\gamma-1)}} \quad (7)$$

The combustion chamber is cylindrical. Its geometry, defined by its length and diameter, is determined using the injector's injection velocity, discharge coefficient, and the residence time of the combustion products within the chamber, as described by Equations (8) through (12):

$$V_{inj}^2 - \frac{C_{d_{inj}}^2 P_c}{2\rho_{prop}} - \frac{120 t_{residence} C_{d_{inj}}^2}{\rho_{prop}} V_{inj} = 0 \quad (8)$$

$$C_{d_{inj}} \approx 0.7 \quad (9)$$

$$t_{res} \approx 0.004(sec) \quad (10)$$

$$\bar{V} \approx 1.5 V_{inj} \quad (11)$$

$$L_c = 1.2\bar{V} t_{res} \quad (12)$$

The approximate volume, total wall surface area, and radius of the combustion chamber are given by Equations (13) through (16), respectively [27]:

$$V_c = A_t\left[L_c\epsilon_c + \frac{1}{3}\sqrt{\frac{A_t}{\pi}}\cot\theta_c\left(\epsilon_c^{1/3}-1\right)\right] \quad (13)$$

$$A_c = 2L_c\sqrt{\pi\epsilon_c A_t} + \csc\theta_c\,(\epsilon_c - 1)A_t \quad (14)$$

$$R_c = \sqrt{\frac{V_c}{\pi L_c}} \quad (15)$$

$$L^* = \frac{V_c}{A_t} \quad (16)$$

The characteristic length of the combustion chamber is typically constrained within a specific range depending on the type of propellant and the desired combustion characteristics. Nozzle parameters can be determined using Equations (17) and (18).

$$V_e = \sqrt{\frac{2g\gamma}{\gamma-1}RT_c\left[1-\left(\frac{P_e}{P_c}\right)^{\frac{\gamma-1}{\gamma}}\right]} \quad (17)$$

$$A_e = \frac{\dot{m}\sqrt{\frac{T_c R}{\gamma}}}{M_e P_c}\left(1+\frac{\gamma-1}{2}M_e^2\right)^{\frac{\gamma+1}{2(\gamma-1)}} \quad (18)$$

The throat geometry is determined using a curved profile with a subsonic radius of curvature of $1.5R_t$, and a supersonic radius of curvature of $\approx 0.382\,R_t$, as shown in Fig. 4.

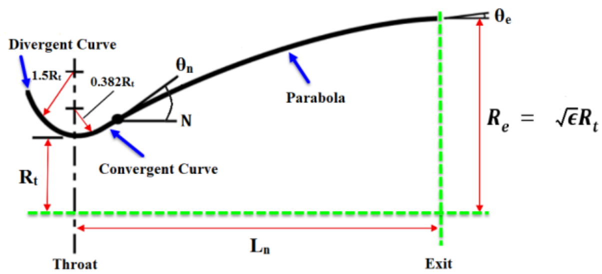

Fig 4. Nozzle geometric schematic [30].

The length of the Rao nozzle, a thrust-optimized contour nozzle, is determined using equation (19), where R_t represents the radius of the nozzle throat.

$$L_n = \frac{0.80(\sqrt{\varepsilon}-1)R_t}{\tan 15°} \quad (19)$$

According to Fig. 4, a Rao nozzle consists of a convergent curve, a divergent curve, and a parabolic curve [31]. First, to find the convergent curve, the X and Y coordinates are obtained according to equations (20) and. (21).

$$x_{conv} = cos(\theta_{conv})\,1.5R_t \quad (20)$$

$$y_{conv} = sin(\theta_{conv})\,1.5R_t + (1.5R_t + R_t) \quad (21)$$

Then, to find the divergent curve, parameters of x and y will be obtained according to the geometry of Fig. 3 and equations (22) and (23), respectively.

$$x_{div} = cos(\theta_{div})\, 0.382R_t \tag{22}$$
$$y_{div} = sin(\theta_{div})\, 1.5R_t + (1.5R_t + R_t) \tag{23}$$

Finally, in order to find the parabolic curve, the following equations are used (equations (24) and (25)):

$$x_{parabola} = ay^2 + by + c \tag{24}$$
$$y_{parabola} = \sqrt{\varepsilon}R_t \tag{25}$$

The constant coefficients a, b, and c in the above equations are obtained using nonlinear geometric relations of the following matrix (equation (26)):

$$\begin{bmatrix} a \\ b \\ c \end{bmatrix} = \begin{bmatrix} y_{div}^2 & y_{div} & 1 \\ y_{exit}^2 & y_{exit} & 1 \\ 2y_{div} & 1 & 0 \end{bmatrix} \begin{bmatrix} y_{div} \\ y_{exit} \\ \dfrac{1}{tan\,\theta_n} \end{bmatrix} \tag{26}$$

It should be noted that the exit angle θ_{exit} will be obtained using the following equation (27):

$$\theta_{exit} = \tan^{-1}\left(\frac{\Delta Y}{\Delta X}\right) \tag{27}$$

Thrust mass (equation (28)) is the sum of the masses of the combustion chamber, nozzle, injector, and cap.

$$M_{thruster} = m_{comb} + m_{nozzle} + m_{inj} + m_{cap} \tag{28}$$

3.1.2. Propellant tanks

The propellant volume is calculated based on the density at specific temperatures. The standard temperature of 20°C is used for storable propellants. Boiling point conditions at ambient pressure are used for cryogenic propellants. Ullage volume calculations should lead to changes in propellant volume due to temperature changes and tank deformation during pressurization. Fuel tanks and oxidizer tanks are placed in a series layout in the body and separated by a common bulkhead. Cylindrical geometry with elliptical caps is used. To calculate the volume, surface area, and weight of the cap, equations (29) to (46) are used [27]:

$$(V_e)_{cap} = \frac{2\pi a^2 b}{3} \tag{29}$$
$$(A_e)_{cap} = a^2 + \frac{\pi b^2 \ln\left[\frac{(1+e)}{(1-e)}\right]}{2e} \tag{30}$$
$$e = \frac{\sqrt{a^2 - b^2}}{a} \tag{31}$$
$$(W_e)_{cap} = \frac{\pi a^2 t_e E' \rho}{2k} \tag{32}$$
$$E' = 2k + \frac{1}{\sqrt{k^2-1}} \ln\left(\frac{k + \sqrt{k^2-1}}{k - \sqrt{k^2-1}}\right) \tag{33}$$

To calculate the volume, surface area, and weight of the cylindrical parts, equations (34) to (36) are used [27]:

$$V_c = \pi a^2 l_c \tag{34}$$
$$A_c = 2\pi a l_c \tag{35}$$
$$W_c = 2\pi a l_c t_c \rho \tag{36}$$

3.2. Feeding system discipline

The feeding system discipline includes the pressurant gas and pressurant tank, valves, and lines. In the self-pressurizing system, the gas used to compress the propellant is the same as the propellant and is in the liquid phase (in pressure equilibrium). To store the propellants in this case, two very significant values must be considered: critical pressure and supercritical pressure. Critical pressure (equation (37)) is the pressure that is in saturation in the pressures of less than that fluid and starts to boil with the fluid pressure reduction to compensate for pressure reduction. Supercritical pressure is the pressure at which all gas becomes liquid, or in other words, there is no gas above this pressure. Since each gas in the liquid phase has a constant density, using the complete gas relation, the supercritical pressure of the desired gas can be obtained.

$$P_{critical} = \rho_{liquid} R_{gas} T_{gas} \tag{37}$$

Pressure ratio (B) is the ratio of initial pressure to final pressure or the ratio of final ullage volume to initial ullage volume (equations (38) to (40), respectively) [32]:

$$B = \frac{P_{gi}}{P_{gf}} = \frac{V_{gf}}{V_{gi}} \tag{38}$$
$$V_{gf} = \frac{V_u}{B-1} \tag{39}$$
$$V_{gi} = \frac{W_u}{\rho(B-1)} \tag{40}$$

The fluid pressure at the beginning and end of the operation should not be higher than the supercritical pressure and less than the critical pressure, respectively. Propellants and pressurant gas specifications are presented in Table 2:

Table 2. Specifications of propellants and pressurant gas.

Fluid	Methane (CH_4)	Oxygen (O_2)	Helium (He)
Critical pressure (bar)	45.99	50.43	2.3
Critical temperature (K)	19.56	154.58	2.15
Gas constant (J/kg.K)	518.28	259.84	2077.1
Density (kg/m^3)	422.6	1141	124.97
Supercritical pressure (bar)	648.64	878.02	-

The tank pressure at the end of the operation is equal to equations (41) and (42):

$$(P_{tank})_{end} = P_{comb} + \Delta P_{lost} \tag{41}$$
$$\Delta P_{lost} = \Delta P_{inj} + \Delta P_{line} + \Delta P_{cool} \tag{42}$$

Approximate values of the pressure drop in the feeding path, including pressure drop in the injector, lines/ pipes, and cooling system, are presented according to [33, 34] in equations (43) to (45).

$$\Delta P_{inj} \approx 0.075 P_c \quad (43)$$

$$\Delta P_{line} \approx 0.075 P_c \quad (44)$$

$$\Delta P_{cool} \approx 0.15 P_c \quad (45)$$

The mass of valves is calculated approximately [33, 34] from equation (46).

$$M_{valve} = 0.07 T^{0.7} + P_c^{0.5} \quad (46)$$

The mass of the pressurant gas is expressed by the following equations (47) to (49):

$$(m_{gas})_f = \frac{(P_{tank})_f}{R_{gas} T_{tank}} (V_{tf} - V_{gtf}) \quad (47)$$

$$(m_{gas})_{ox} = \frac{(P_{tank})_{ox}}{R_{gas} T_{tank}} (V_{tox} - V_{gtox}) \quad (48)$$

$$M_{gas} = (m_{gas})_f + (m_{gas})_{ox} \quad (49)$$

3.3. Structure discipline

In the structural discipline, the thickness of the structures is predicted. The design of the finset, skirt, fairing, and body shell is done according to the load factors. The structural thickness of the combustion chamber, nozzle, propellant, and pressurant tanks is obtained from equations (50) to (53). In order to determine the thickness of the combustion chamber structure, in addition to the effect of pressure, the effect of thrust force must also be applied.

$$\delta_{comb} = \frac{n_{SF}}{2 S_{str}} \left(\frac{\pi R_c^2 P_c + T}{\pi R_c} \right) \quad (50)$$

$$\delta_{nozzle} = \frac{n_{SF}}{2 S_{str}} (P_c R_c + P_e R_e) \quad (51)$$

$$\delta_{tank}^{cyl} = \frac{n_{SF}}{S_{str}} (P_{tank} R_{tank}) \quad (52)$$

$$\delta_{tank}^{sph} = \frac{n_{SF}}{2 S_{str}} (P_{tank} R_{tank}) \quad (53)$$

The tanks use an aluminum liner and carbon fiber coating. The physical characteristics of these two types of materials are summarized in Table 3.

Table 3. Physical characteristics of aluminum and carbon composite.

Structure	Young's modulus (GPa)	Elastic module (MPa)	Density (kg/m^3)
Aluminum	69	400	2700
Carbon Composite	530	–	1800

The structural mass includes the mass of the fairing, shell (first stage, second stage, and interstage), finset, and skirt, as detailed in equation (54). For a more in-depth analysis of structural design, refer to Reference [27].

$$M_{structure} = M_{bodyshell} + M_{fairing} + M_{fin} + M_{skirt} \quad (54)$$

3.4. Aerodynamic discipline

Missile-DATCOM was used to analyze and extract aerodynamic coefficients. Inputs to this software include flight conditions, Mach number (M), angle of attack (α), and altitude (H), reference area (S_{ref}), reference length (L_{ref}), and geometric parameters. The outputs are aerodynamic coefficients, with the most critical being the pitching moment coefficient (C_m), which must be negative throughout all flight regimes to ensure stability.

3.5. Trajectory and pitch program discipline

The trajectory simulation task involves simulating the LV's flight from launch to satellite injection into orbit. This process determines the feasibility of achieving the desired orbit by solving the equations of motion. To ensure optimal performance and trajectory, the simulation requires a pitch program, which is determined by an internal optimizer (see Figure 5).

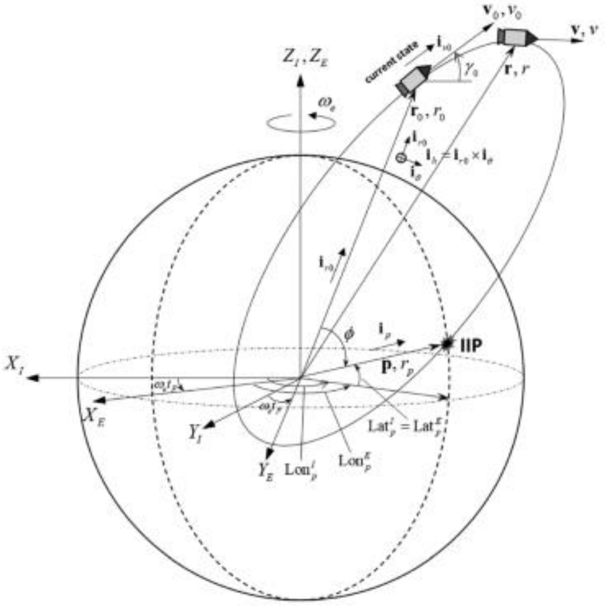

Fig 5. Forces entering the LV in flight.

To analyze the trajectory, a 3-DOF simulation of the following equations is governed by equations (55) to (58).

$$T = \dot{m} v_e + (P_e - P_a) A_e \quad (55)$$

$$L = \frac{1}{2} \rho V^2 S C_{L_\alpha} \alpha \quad (56)$$

$$D = \frac{1}{2} \rho V^2 S C_D \quad (57)$$

$$g = \frac{\mu}{r^2} \quad (3.9862 \times 10^4 \ m^3/s^2) \quad (58)$$

Position, velocity vectors, and Mach number can be calculated from equations (59) to (61), respectively:

$$r = \sqrt{x^2 + y^2} \tag{59}$$

$$V = \sqrt{V_x^2 + V_y^2} \tag{60}$$

$$M = \frac{V}{a} \tag{61}$$

The flight path angle, range angle, and angle of attack can also be obtained from equations (62) to (64), respectively:

$$\gamma = \sin^{-1}\left(\frac{V_y}{V}\right) + \beta \tag{62}$$

$$\beta = \sin^{-1}\left(\frac{x}{r}\right) \tag{63}$$

$$\alpha = \theta - \gamma \tag{64}$$

Finally, the equations of motion are proposed as (65) to (68):

$$\dot{V}_x = \frac{1}{M_{LV}}[-M_{LV}g\sin(\beta) - D\cos(\gamma-\beta) - L\sin(\gamma-\beta) + T\cos(\theta-\beta)] \tag{65}$$

$$\dot{V}_y = \frac{1}{M_{LV}}[-M_{LV}g\cos(\beta) - D\sin(\gamma-\beta) + L\cos(\gamma-\beta) + T\cos(\theta-\beta)] \tag{66}$$

$$\dot{x} = V_x \tag{67}$$

$$\dot{y} = V_y \tag{68}$$

Generally, the pitch program is introduced in Fig. 6 with three main parts, including the vertical phase, quadratic phase, and linear phase.

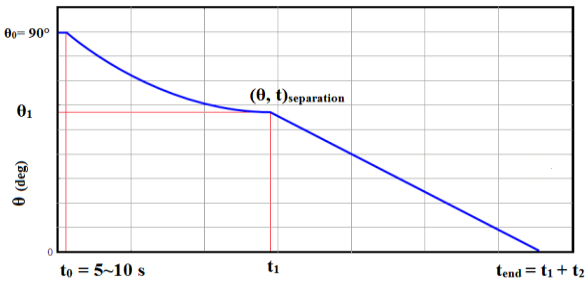

Fig 6. Typical pitch program for a two-stage LV.

To determine the pitch program angle, based on the equations mentioned in equations (69) and (70), it is necessary to specify parameters such as the separation angle of the first and second stages and the injection angle in orbit. By knowing the amount of burning time of the first and second stages, the pitch program angle can be extracted, which can be used in simulation equations.

$$\theta = \frac{(\theta_0 - \theta_1)}{\left(t_{burn_1} - t_0\right)^2}\left(t_{burn_1} - t\right)^2 + \theta_1 \tag{69}$$

$$\theta = \theta_1 + \left(\frac{\theta_1}{t_{end} - t_{burn_1}}\right)\left(t_{burn_1} - t\right) \tag{70}$$

Final constraints on trajectory are related to orbit parameters as follows in equation (71):

$$\begin{aligned} H_{LV} &\geq H_{orbit} \\ V_{LV} &\geq V_{orbit} \end{aligned} \tag{71}$$

4 Multidisciplinary Design Optimization Framework

Various optimization methods have been employed for the optimum design of turbopump LVs [35, 36], but nothing has been found on optimizing pressure-fed LVs so far. This paper is the first time that develop a multidisciplinary optimization design algorithm for a pressure-fed LV. As mentioned earlier, the LV configuration is a two-stage rocket. A hybrid optimizer that includes a genetic algorithm (GA) and sequential quadratic programming (SQP) has been used to derive the global optimum solution.

AAO is the most basic MDO technique and is widely accepted by the industry. In AAO, control is given to a system-level optimizer that ensures a global objective is met by having a single designer control the entire system. AAO solves the global MDO problem by moving all local-level design variables and constraints away from each discipline to a new system-level optimizer entrusted with optimizing a global objective. High feasibility in solution is one of the advantages of AAO. Using the AAO method provides highly improved final results without any costly iterative system analysis. On the other hand, because the basis of the work is a feasibility study of an LV with a pressure-fed propulsion system, the basic MDO method in which process control is left to the system-level optimizer is selected. Also, based on the results extracted in [30], the convergence and simplicity of this approach (AAO) are another reason for selection. Variables, parameters, constraints, variable boundaries, and cost functions are summarized as follows:

$$Design\ variables: \begin{cases} M_{pay} & r_{tank_{ox}} & r_{tank_{fuel}} & \theta_{staging} \\ t_{burn_1} & t_{burn_2} & OF_1 & OF_2 \end{cases}$$

$$Design\ parameters: \begin{cases} H_{orbit} & V_{orbit} & \gamma_{orbit} & i_{orbit} & \Phi_{launchsite} \\ (T_{eng})_1 & (T_{eng})_2 & (N_{eng})_1 & (N_{eng})_2 & N_{fin} \\ (P_c)_1 & (P_c)_2 & \rho_{ox} & \rho_{fuel} & \rho_{str} \\ \theta_{nose} & (\theta_n)_{nozz} & \theta_c & t_{gtank_{liner}} & h_{pay} \end{cases}$$

$$Design\ constraints: \begin{cases} C_1: 6 < \dfrac{L_{LV}}{D_{LV}} < 16 \\ C_2: 5 < \dfrac{L_{stage_1}}{D_{stage_1}} < 12 \\ C_3: 3 < \dfrac{L_{stage_2}}{D_{stage_2}} < 5.5 \\ C_4: D_{stage_i} \geq D_{eng\_noz_i} \\ C_5: n_1 \geq 1.2\ ; \quad n_2 \geq 0.5 \\ C_6: H_{orbit} - H_{LV} \leq 10^{-5} \\ C_7: V_{orbit} - V_{LV} \leq 10^{-5} \\ C_8: \theta_1 - \theta_s \leq 10^{-4} \end{cases}$$

$$Variable\ limitations: \begin{cases} variable & L\,b & Ub \\ M_{pay} & 50 & 3000 \\ OF_1 & 2.0 & 3.8 \\ OF_2 & 2.0 & 3.8 \\ t_{burn_1} & 90 & 200 \\ t_{burn_2} & 100 & 400 \\ r_{tank} & 0.5 & 1.5 \end{cases}$$

$$Cost\ function: C.F = \mu_{pay} = \frac{M_{pay}}{M_{LV}}$$

The design structure matrix (DSM) of the two-stage LV based on the AAO framework has been illustrated in Fig. 7.

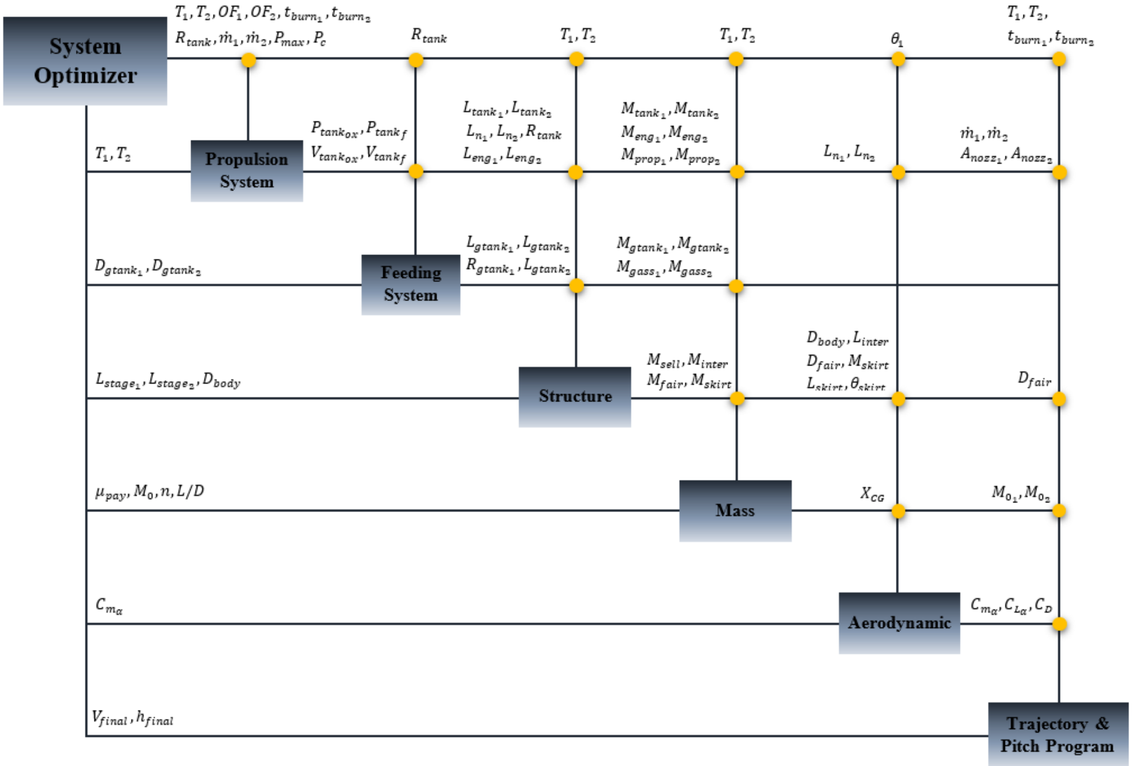

Fig 7. Design Structure Matrix (DSM) of LV based on AAO framework.

The main parameters of the adjusted optimizer are presented in Table 4.

Table 4. Adjusted parameters of the optimizer.

SQP Algorithm	
Max Iteration	200
Function Tolerance	1e-10
X Tolerance	1e-10
GA Algorithm	
Initial population	100
Generations	20
Stall Generation Limit	10
Cross-over Function	0.7
Elite Count	5

The mentioned adjustments were derived during the optimization process specifically for this study and may vary for similar research.

5 VALIDATION OF MULTIDISCIPLINARY DESIGN OPTIMIZATION ALGORITHM

According to the literature review, complete information and data are not available for a case study. Therefore, it was practically impossible to validate the results directly for the entire LV. Due to the lack of information, two steps have been implemented for validation. In the first step, the propulsion model will be evaluated by an existing case study (Leon-1), and in the second step, a redesign of a stage (Falcon-1 due to the similarity in the use of a pressurized tank and propulsion system) has been done [30]. The specifications of the Leon-1 engine are provided in Table 5.

Table 5. Specifications of Leon-1 MethaLox engine [37].

Some Specifications of the Leon-1 Engine			
Thrust (kN)	9	Burn time (s)	10
Chamber pressure (bar)	72	Propellant	CH_4/O_2
Specific length (cm)	90	θ_c	40
Isp (s)	300	ε_c	5.25

Evaluation of the results of the MethaLox pressure-fed thruster designed by the proposed algorithm and the case study of Leon-1 [37] has been done in Table 6.

Table 6. Evaluation of proposed algorithm modeling and case study (Leon-1)

Parameter	Leon-1 engine	Proposed Model	err
Nozzle expansion ratio	9.22	9.718	5.40%
Chamber diameter (cm)	7.318	7.244	1.00%
Nozzle exit diameter (cm)	9.702	9.857	1.60%
Throat diameter (cm)	3.184	3.162	0.71%
Chamber length (cm)	17.719	17.142	3.26%

According to Table 6, the maximum errors are below 6%, which is acceptable for preliminary design phases. Table 7 presents the specifications of the pressure-fed Kestrel engine used in the Falcon-1 rocket, as reported in References [38, 39, 20].

Table 7. Kestrel thruster specifications.

Some Specifications of the Kestrel Engine of Falcon-1 LV		
Thrust	$T\ (kN)$	33.361
Mixture ratio	OF	2.36
Chamber pressure	$P_c\ (bar)$	9.3
Specific impulse	$I_{sp}\ (s)$	327
Burn time (s)	t_{burn}	378
Nozzle area ratio	ε	60
Propellant	KeroLox (RP-1/O_2)	
Angle of the combustion chamber	θ_c	40.5°
Angle of nozzle	θ_n	35.7°

The stage redesign, including propellant tanks, was conducted using the proposed algorithm and compared to the Falcon-1 configuration in Table 8.

Table 8. Validation of Falcon-1 and proposed algorithm.

Parameter	Falcon-1 (2nd stage)	LV designed	Error Percent
$I_{sp}\ (s)$	327	323	1.22%
$\dot{m}_{eng}(^{kg}/_{s})$	10.399	10.5328	1.28%
ε	60	61.4	2.33%
$(A_e)_{nozz}(m^2)$	1.3305	1.2081	9.19%
$m_{eng}(kg)$	52	55.94	7.57%
$M_{prop}(kg)$	3931.2	3981.4	1.27%
$m_{ox}(kg)$	2694.8	2796.4	3.77%
$m_{fuel}(kg)$	1141.7	1184.9	3.78%
$m_{He}(kg)$	9.8	10.4	6.12%

According to Table 8, the maximum error is less than 10%, which is considered acceptable for preliminary design.. This suggests that the accuracy of the modeling for pressurized propulsion systems is suitable.

6 MULTIDISCIPLINARY DESIGN OPTIMIZATION OF LV WITH NON-TURBOPUMP PROPULSION SYSTEM

As mentioned earlier, the mission objective for both LVs is to maximize the payload mass (max μ_{pay}) to orbit (250 km) while minimizing the overall gross mass, subject to the specified constraints and limitations.

6.1. SPF-LV design

Multidisciplinary design optimization of the SPF-LV was conducted using the AAO framework. The results indicate that this configuration, relying solely on a self-pressurized propulsion system for both stages, is unable to achieve a 250 km orbit with any payload. Table 9 presents the results of the optimized SPF-LV design.

Table 9. Optimum design result of the SPF-LV.

Parameter		Value
Take-off gross mass (kg)	M_{LV}	85161.25
Payload mass (kg)	$M_{payload}$	0.00
Payload mass ratio	μ_{pay}	0.00
Different altitudes of the orbit and launcher (km)	err_h	0.00019
Different velocities of the orbit and launcher (m/s)	err_v	-286.32
Launcher length(m)	L_{LV}	38.84
First stage gross mass (kg)	$(m_0)_1$	76638.3
Second stage gross mass (kg)	$(m_0)_2$	8393.9
First stage diameter (m)	$(D_{stage})_1$	2.43
Second stage diameter(m)	$(D_{stage})_2$	2.43
First stage length (m)	$(L_{stage})_1$	28.11
Second stage length (m)	$(L_{stage})_2$	3.63
Propellant mass of 1st stage (kg)	$(M_{propellant})_1$	71171.6
Propellant mass of 2nd stage (kg)	$(M_{propellant})_2$	7449.8
Thrust of 1st stage engine (kN)	T_1	1350
Thrust of 2nd stage engine (kN)	T_2	150
Specific impulse of 1st stage engine (s)	Isp_1	291.19
Specific impulse of 2nd stage engine (s)	Isp_2	363.87
Burn time of 1st stage engine (s)	$(t_{burn})_1$	132.5
Burn time of 2nd stage engine (s)	$(t_{burn})_2$	156
1st stage Deadgas fuel mass (kg)	$\left(M_{dead_f}\right)_1$	2805.03
1st stage Deadgas oxidizer mass (kg)	$\left(M_{dead_{ox}}\right)_1$	5724.64
2nd stage Deadgas fuel mass (kg)	$\left(M_{dead_f}\right)_2$	290.04
2nd stage Deadgas oxidizer mass (kg)	$\left(M_{dead_{ox}}\right)_2$	601.97

As indicated by the results, the optimal LV is not capable of reaching the velocity of the destination orbit. The optimum velocity is 286.32 m/s, smaller than the velocity of the destination orbit. Table 9 presents the results of the optimal solution of SPF-LV.

6.2. GPF-LV Design

Using the AAO framework, the optimum GPF-LV has been derived, and it is feasible.

The optimum results of GPF-LV are presented in Table 10.

Table 10. Optimum design results of the GPF-LV

Parameter		Value
Take-off gross mass (kg)	M_{LV}	85601.93
Payload mass (kg)	$M_{payload}$	1857.35
Payload mass ratio	μ_{pay}	0.02169
Different altitudes of the orbit and launcher (km)	err_h	-0.00018
Different velocities of the orbit and launcher (m/s)	err_v	0.00000
Launcher length(m)	L_{LV}	39.63
First stage gross mass (kg)	$(m_0)_1$	70367.18
Second stage gross mass (kg)	$(m_0)_2$	13207.96
First stage diameter (m)	$(D_{stage})_1$	2.654
Second stage diameter(m)	$(D_{stage})_2$	2.654
First stage length (m)	$(L_{stage})_1$	25.70
Second stage length (m)	$(L_{stage})_2$	5.71
Propellant mass of 1st stage (kg)	$(M_{propellant})_1$	64798.04

Parameter		Value
Propellant mass of 2nd stage (kg)	$(M_{propellant})_2$	11850.16
1st stage Fuel mass (kg)	$(M_{fuel})_1$	18701.87
1st stage Oxidizer mass (kg)	$(M_{oxidizer})_1$	46096.17
2nd stage Fuel mass (kg)	$(M_{fuel})_2$	3094.52
2nd stage Oxidizer mass (kg)	$(M_{oxidizer})_2$	8755.64
1st stage Helium mass for fuel (kg)	$(M_{pressgas_f})_1$	626.32
1st stage Helium mass for oxidizer (kg)	$(M_{pressgas_{ox}})_1$	573.059
2nd stage Helium mass for fuel (kg)	$(M_{pressgas_f})_2$	115.99
2nd stage Helium mass for oxidizer (kg)	$(M_{pressgas_{ox}})_2$	120.84
Thrust of 1st stage engines (kN)	T_1	1350
Thrust of 2nd stage engine (kN)	T_2	150
Specific impulse of 1st stage engine (s)	Isp_1	291.386
Specific impulse of 2nd stage engine (s)	Isp_2	363.790
Burn time of 1st stage engine (s)	$(t_{burn})_1$	137.149
Burn time of 2nd stage engine (s)	$(t_{burn})_2$	281.826
Skirt mass (kg)	M_{skirt}	36.05
Skirt length (m)	L_{skirt}	1.329
Skirt diameter (m)	D_{skirt}	3.466
Skirt sweep angle (deg)	$(\theta_{sweep})_{skirt}$	73.02
Finset mass (kg)	M_{finset}	83.29
Fin length (m)	S_{fin}	0.812

According to the results, GPF-LV weighs about 85.6 tons and carries an 1857 kg payload to a 250 km orbit. It is clear that this type of LV can reach a higher orbit with a lower payload mass or can send a lower payload mass with a lower total LV mass into 250 km. As can be seen from the design results of these two LVs, unlike the SPF-LV, which was not feasible, the GPF-LV provided acceptable results. Considering the feasibility of GPF and the infeasibility of SPF and knowing the lower cost and complexity of the SPF structure compared to GPF, it may be possible to implement a combination of these two types of propulsion systems in one launch vehicle. Although its efficiency is lower than GPF, it has relatively less cost and complexity and is structurally more affordable, so it is probable. For these reasons, a mixed-stage LV, including GPF and SPF, can be designed.

6.3. Mixed-stages LV (GPF-SPF-LV) design

After reviewing the multidisciplinary design optimization results, the idea of combining these two propulsion systems into a mixed-stage LV emerged. After optimization, it was recognized that only one configuration was feasible. The feasible configuration included the first stage being a gas-pressure type and the second stage being a self-pressure type. Changing the selection of stage type led to infeasible solutions.

The results of this design are presented below.

The optimum design results for the GPF-SPF-LV are summarized in Table 11.

Table 11. Optimum design result of the GPF-SPF-LV

Parameter		Value
Take-off gross mass (kg)	M_{LV}	83066.1
Payload mass (kg)	$M_{payload}$	670
Payload mass ratio	μ_{pay}	0.00807
Different altitudes of the orbit and launcher (km)	err_h	-0.00015
Different velocity of the orbit and launcher (km/s)	err_v	0.0000
Launcher length(m)	L_{LV}	36.964
First stage gross mass (kg)	$(m_0)_1$	75911.59
Second stage gross mass (kg)	$(m_0)_2$	6362.32
First stage diameter (m)	$(D_{stage})_1$	2.636
Second stage diameter(m)	$(D_{stage})_2$	2.636
First stage length (m)	$(L_{stage})_1$	27.85
Second stage length (m)	$(L_{stage})_2$	2.89
Propellant mass of 1st stage (kg)	$(M_{propellant})_1$	69865.94
Propellant mass of 2nd stage (kg)	$(M_{propellant})_2$	5505.07
Thrust of first engine (kN)	T_1	1350
Thrust of 2nd stage engine (kN)	T_2	150
Specific impulse of 1st stage engine (s)	Isp_1	291.64
Specific impulse of 2nd stage engine (s)	Isp_2	362.89
Burn time of 1st stage engine (s)	$(t_{burn})_1$	148.00
Burn time of 2nd stage engine (s)	$(t_{burn})_2$	115.01
1st stage Fuel mass (kg)	$(M_{fuel})_1$	19654.59
1st stage Oxidizer mass (kg)	$(M_{oxidizer})_1$	50211.35

Parameter		Value
2nd stage Fuel mass (kg)	$(M_{fuel})_2$	1225.62
2nd stage Oxidizer mass (kg)	$(M_{oxidizer})_2$	3622.13
1st stage Helium mass for fuel (kg)	$(M_{pressgas_f})_1$	656.97
1st stage Helium mass for oxidizer (kg)	$(M_{pressgas_{ox}})_1$	622.39
2nd stage Deadgas fuel mass (kg)	$(M_{dead_f})_2$	206.49
2nd stage Deadgas oxidizer mass (kg)	$(M_{dead_{ox}})_2$	450.84
Skirt mass (kg)	M_{skirt}	18.767
Skirt length (m)	L_{skirt}	0.738
Skirt diameter (m)	D_{skirt}	3.095

Parameter		Value
Skirt sweep angle (deg)	$(\theta_{sweep})_{skirt}$	72.312
Finset mass (kg)	M_{finset}	211.105
Fin length (m)	S_{fin}	0.864

According to the results, the optimum GPF-SPF-LV has a mass of approximately 83.1 tons and can carry a payload of 670 kg to a 250 km orbit. It should be noted that this type of LV can reach a higher orbit with a lower payload mass or can send a lower payload mass to a 250 km orbit with a lower gross mass.

6.4. Comparison of SPF, GPF, and GPF-SPF LVs

The optimum solution geometries of LVs are shown in Fig. 8.

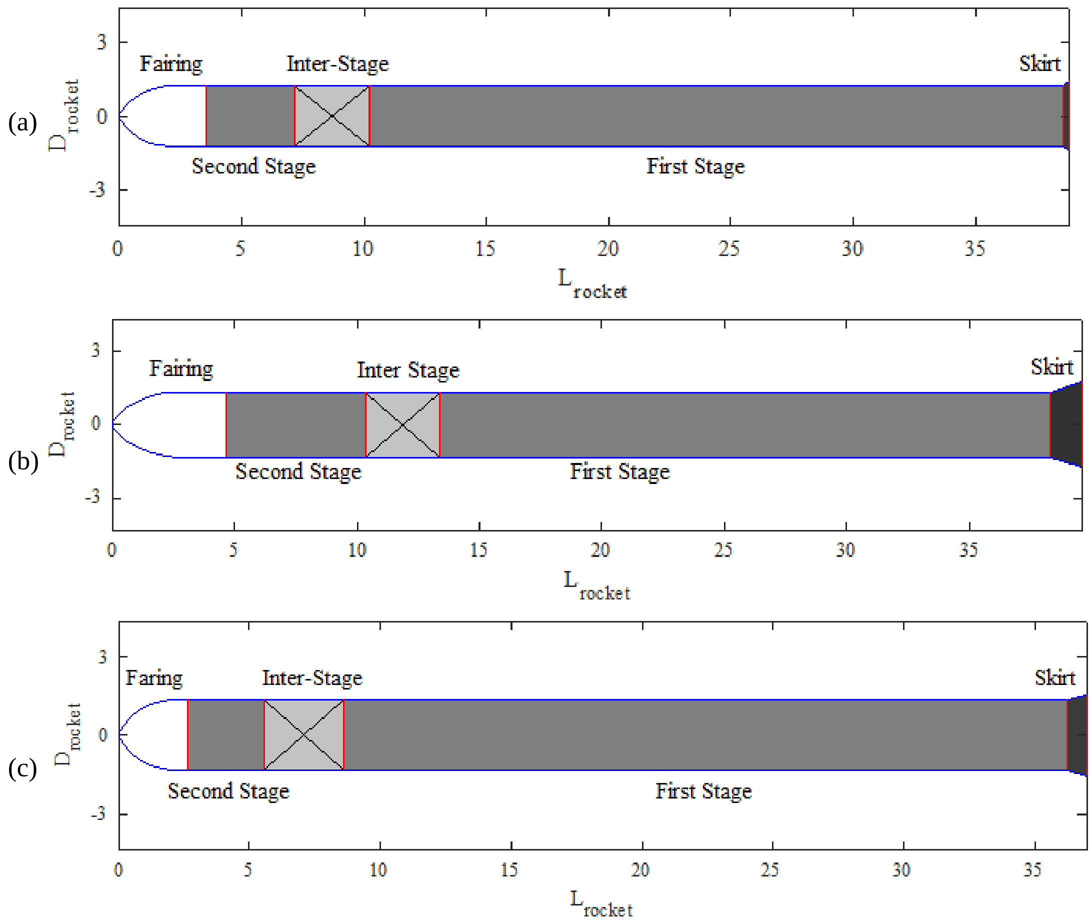

Fig 8. MD schematic designs: a) SPF-LV, b) GPF-LV, and c) GPF-SPF-LV.

Fig 9 shows diagrams of altitude, velocity, thrust, rocket mass, slant range, and the optimal pitch program for the SPF-LV, GPF-LV, and GPF-SPF-LV.

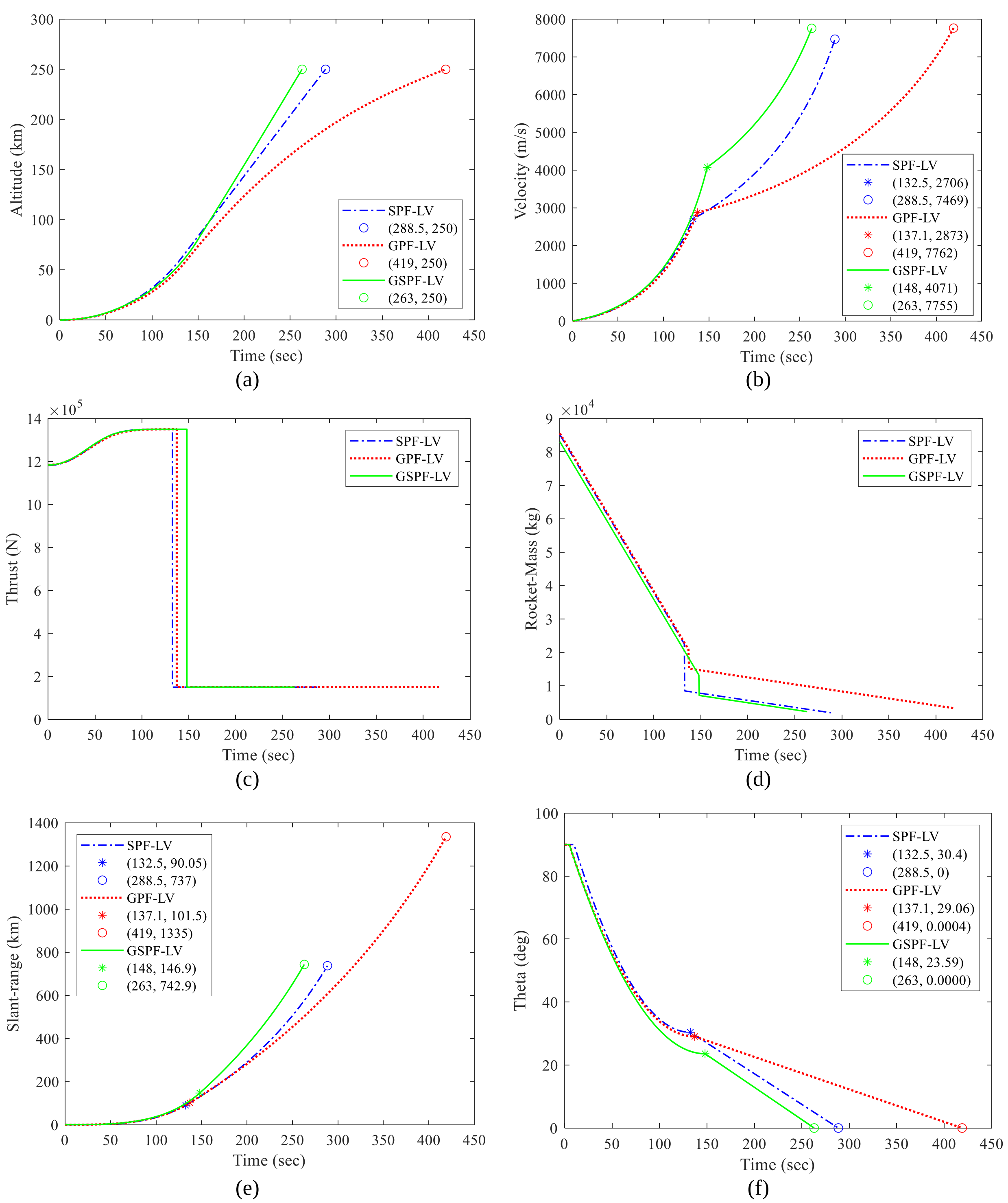

Fig 9. Graphs of pressure-fed launch vehicles: a) altitude, b) velocity, c) thrust, d) rocket mass, e) slant range, and f) optimum pitch program.

As indicated by the results, and also in Figures 9(a) and 9(b), while all three launch vehicles reached orbital altitude, the optimal SPF-LV could not achieve the required velocity for the destination orbit. It fell short by 286.32 m/s. This suggests that this type of propulsion system may need further technological advancements, but it could be suitable for suborbital missions. In contrast, the GPF-LV and GPF-SPF-LV reached velocities of 7762 and 7755 m/s, respectively.

In Figure 9(c), all three launch vehicles exhibit similar thrust profiles, with only minor differences in thrust levels during a brief period around the separation point.

As shown in Figure 9(d), the first stages of all three LVs have similar mass profiles. Additionally, the second stages of the SPF-LV and GPF-SPF-LV exhibit similar mass trends. However, the GPF-LV's second stage has a distinct mass profile compared to the other two.

While the mixed-stage LV solution offers lower performance compared to the GPF-LV, it might also be less costly. To theoretically support this claim, another GPF-LV with the same mission parameters (670 kg payload to a 250 km orbit) was designed, and its mass, dimensions, and cost are presented in Table 12.

Table 12. Validation of mass, dimensional, and cost results from the comparison of two GPF-SPF-LV and GPF-LV (for the same mission).

Launch vehicle	**Mass (tons)**		**Dimensional (m)**			**Cost (k$)**		
	M_{LV}	μ_{pay}	L_{LV}	D_{LV}	$(L/D)_{LV}$	**Propellant**	**Structure**	**Material** (propellant + structure)
GPF-SPF-LV	83.0661	0.00807	36.964	2.636	14.023	16.6255	97.0014	113.6269
GPF-LV	53.7146	0.01247	27.154	2.792	9.726	10.7796	73.4467	84.2263
Percentage of improvement	↓ 35.34%	↑ 53.66%	↓ 26.54%	↑ 5.9%	↓ 30.64%	↓ 5.85 k$	↓ 23.55 k$	↓ 25.87%

The results in Table 12 demonstrate the superiority of the GPF-LV over the GPF-SPF-LV in terms of mass, dimensions, and performance. The GPF-LV achieves a 35.3% reduction in gross mass, a 30.6% decrease in size, and a 53.6% increase in mass ratio. Assuming similar construction and production costs for all LV types, the GPF-LV also offers a 25.8% cost reduction in propellant and structural components, making it a more cost-effective and efficient choice. The efficiency and payload capacity of this launcher, determined using MDA, are detailed in Reference [40].

6.5. Sensitivity analysis

To demonstrate the convergence and optimality of the design point, a sensitivity analysis was conducted for variations of ±1% and ±5% on the optimal solution. The results are presented as follows:
The results of the sensitivity analysis for ±1% variations on the optimal solution are presented in Table 13.

Table 13. The sensitivity analysis for ±1% variations

Variables	Optimum values	Variation of CF		Const
		+5%	-5%	
M_{pay}	1857.35 (kg)	0.8982	0.9446	✓
OF_1	2.465	0.0420	0.0486	✓
OF_2	2.829	0.0049	0.0036	✓
$(t_{burn})_1$	137.149 (s)	0.8095	0.8229	✓
$(t_{burn})_2$	281.825 (s)	0.1487	0.1491	✓
r_{tank}	1.315 (m)	0.0162	0.0168	✓
θ_{skirt}	73.02 (deg)	0.0004	0.0004	✓
S_{fin}	0.812 (m)	0.0002	0.0002	✓
L_{skirt}	1.329 (m)	0.0004	0.0004	✓

Based on the results in Table 13, the derived solution is optimum.

The results of the sensitivity analysis for ±5% variations on the optimal solution are presented in Table 14.

Table 14. The sensitivity analysis for ±5% variations

Variables	Optimum values	Variation of CF		Const
		+5%	-5%	
M_{pay}	1857.35 (kg)	4.8861	4.8968	✓
OF_1	2.465	-0.1472	0.3114	✗
OF_2	2.829	0.0363	0.0051	✓
$(t_{burn})_1$	137.149 (s)	3.9208	-4.2544	✗
$(t_{burn})_2$	281.825 (s)	0.7391	0.7502	✓
r_{tank}	1.315 (m)	0.0749	0.0902	✓
θ_{skirt}	73.02 (deg)	-0.0019	0.0022	✗
S_{fin}	0.812 (m)	0.0011	0.0011	✓
L_{skirt}	1.329 (m)	0.0024	0.0024	✓

According to the above table, although some changes in the variables have resulted in improvement in the cost function, some constraints have not been satisfied. Therefore, the derived solution is optimum and feasible.

The percentage variations in the cost function for the sensitivity analysis with ±5% variations are shown in Figure 11.

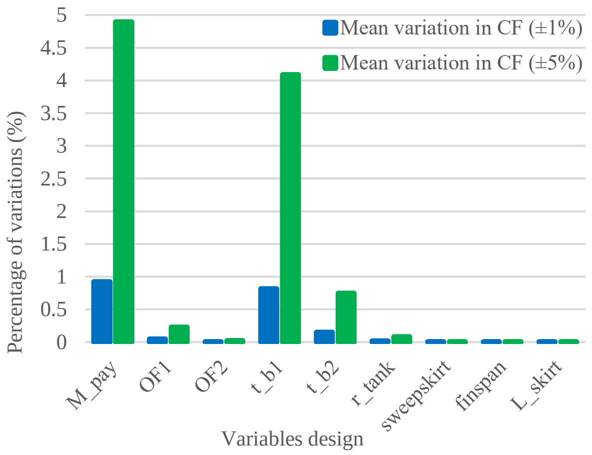

Fig 11. The sensitivity analysis for ±1% and ±5% variations

According to Fig. 11, M_{pay}, $(t_{burn})_1$, and $(t_{burn})_2$ have more effect on the cost function.

In the sensitivity analysis, variations in the variables from the identified optimum values lead to an increase in the cost function, confirming the derived optimal point. Additionally, all constraints are satisfied despite the variations.

CONCLUSION

Using the AAO framework, this paper designed three types of launch vehicles (LVs): SPF-LV, GPF-LV, and GPF-SPF-LV. To validate the non-turbopump propulsion system and LV design modeling, the results of the proposed algorithm were compared with data from the Leon-1 engine and the second stage of the Falcon-1, respectively. This comparison demonstrated that modeling errors (in mass, performance, and dimensions) were less than 9.0% when compared to case study data. Following validation, multidisciplinary design optimization (MDO) of the three LV types (SPF-LV, GPF-LV, and GPF-SPF-LV) was performed using the AAO framework. Optimization results indicate that the optimum SPF-LV, with a total mass of 85,161 kg, could not achieve orbital velocity. In contrast, the optimum GPF-LV, with a total mass of 85,601 kg, can inject a 1,857 kg payload into a 250 km orbit. To combine the performance advantages of GPF-LV with the lower complexity of SPF-LV, a GPF-SPF-LV was developed, featuring a GPF-type first stage and an SPF-type second stage. The optimized GPF-SPF-LV has a total mass of 83,066 kg and can deliver a 670 kg payload to the desired orbit. When comparing the GPF-LV and GPF-SPF-LV designs for the same mission (670 kg payload to a 250 km orbit), the GPF-LV exhibits superior performance: it is 34.5% lighter, 22% shorter, and 52.5% more efficient, and it is also 25.8% more cost-effective due to reduced propellant and structural costs. This research innovates by applying Multidisciplinary Design Optimization (MDO) to a non-turbopump launch vehicle design. This includes investigating three distinct feeding system architectures and their impact on performance, weight, and other relevant design parameters. Integrating aerodynamic stability considerations into the conceptual design phase, including its influence on vehicle geometry and the necessity of a skirt, is another key contribution. The analysis demonstrates the superior performance of the GPF feeding system architecture.

CONFLICT OF INTEREST

No potential conflict of interest was reported by the authors.

REFERENCES

[1]r H. W. Jones, "The Recent Large Reduction in Space Launch Cost", In *48th International Conference on Environmental Systems*, Albuquerque, New Mexico, 2018.

[2] J. M. Bockel, "The Future of the Space Industry," NATO Parliamentary Assembly (Economic and Security Committee (ESC)), France, 2018.

[3] J. Greason, and J.C. Bennett, "The economics of space: An industry ready to launch", *Reason Foundation*, Los Angeles, 2019.

[4] N. Sarzi-Amade, T. Bauer, J. Wertz, and M. Rufer, "Sprite, a very low-cost launch vehicle for small satellites," In *Proceedings of the 12th Reinventing Space Conference*, Springer, pp. 165-178, 2017, https://doi.org/10.1007/978-3-319-34024-1_13

[5] R. Van Allen, T. P. Bauer, S. Chakraborty, S. Collier, P. Graven, J. Hansen, H. F. Messinger, and J. R. Wertz, "Responsive, Low-Cost Access to Space with ELVIS- an Expendable Launch Vehicle with Integrated Spacecraft," In *17 Annual USU/AIAA Small Satellite Conference*, 2003.

[6] R. Conger, J. Wertz, and J. Kulpa, "The Scorpius Expendable Launch Vehicle Family and Status of the Sprite Mini-Lift," In *20th AIAA International Communication Satellite Systems Conference and Exhibit*, Montreal, Quebec, Canada, 2002.

[7] S. Chakroborty and T. Bauer, "Using pressure-fed propulsion technology to lower space transportation costs," In *40th AIAA/ASME/SAE/ASEE Joint Propulsion Conference and Exhibit*, Lauderdale- Florida, *AIAA*, p. 3358, 2012, https://doi.org/10.2514/6.2004-3358

[8] H. Naseh, M. MirShams, and H.R. Fazeley, "Surrogate Based Simulation in Multidisciplinary Design Optimization of a Space Transportation System", *Journal of Aerospace Science and Technology*, vol. 15, issue 2, pp-1-15, 2022, 10.22034/jast.2022.329569.1115.

[9] Armbrust, E., "Liquid Engine External Pressurizer (LEEP)", M.Sc. thesis, Williams Honors College, Honors Research Projects. 1559, 2022.

[10] H. R. Alimohammadi, H. Naseh, and Ommi, F., "An integrated methodology applied for reliability-based multidisciplinary design optimization in EPFE with LOX/kerosene", *Reliability Engineering & System Safety*, vol. 240, Art. No. 109570, 2023, 10.1016/j.ress.2023.109570

[11] L. Baraton, A. Urbano, L. Brevault, and M. Balesdent, "Comparative review of Multidisciplinary Design Analysis and Optimization architectures for the preliminary design of a liquid rocket engine", in *Aerospace Europe Conference 2023–10th EUCASS–9th CEAS*, Lausanne, Switzerland, HAL open science, 2023, 10.13009/EUCASS2023-834.

[12] C. Joyner, Whitney Rocketdyne, D. Levack, R. Rhodes, John W. C. Robinson "Propulsion System Choices and Their Implications," In *46th AIAA/ASME/SAE/ASEE Joint Propulsion Conference & Exhibit*, Nashville, Tennessee, p. 6506, 2010, 10.2514/6.2010-6506.

[13] Cen, J. and Xu, J., "A new prototype of the self-pressurizing fuel tank for micro and nano-satellites," *Acta Astronautica*, vol. 64, no. 4, pp. 410-415, 2009, https://doi.org/10.1016/j.actaastro.2008.09.012.

[14]"Morpheus lander," https://www.nasa.gov/centers/marshall/news/releases/nasa-tests-methane-powered-engine-components-for-next-generation-landers, NASA, 2015.

[15] S. Stanley, "Preliminary Design of a Pressurization System for Small Bipropellant Rocket Engines", Ph.D. dissertation, Texas Univ., Arlington, 2011.

[16] J. S. Matsumoto, H. Igoh Okaya, and J. Kawaguchi, "Concept of a self-pressurized feed system for liquid rocket engines and its fundamental experiment results", *Acta Astronautica*, vol. 133, pp. 166-176, 2017, https://doi.org/10.1016/j.actaastro.2017.01.017.

[17] J.S. Parks, "Practical Applications of Pressure-Fed LOX/CH4 Rocket Engines", Ph.D. dissertation, Texas Univ., El Paso, 2022.

[18] E.A. Hurlbert, M.J. Atwell, J.C. Melcher, and R. L. Morehead, "Integrated Pressure-Fed Liquid Oxygen/Methane Propulsion Systems-Morpheus Experience, MARE, and Future Applications," In *52nd AIAA/SAE/ASEE Joint Propulsion Conference*, Art. No. 4681, 2016, https://doi.org/10.2514/6.2016-4681.

[19] M. Hashemi Doulabi, H. Darabi, and J. Roshanian, "Comparison Between Traditional Method (Statistical Method) and Multidisciplinary Optimization Method (AAO) in Designing of a Lightweight Liquid Propellant LV," *Journal of Space Science and Technology*, vol. 5, no. 1, pp. 61-72, 2012, (in Persian).

[20] "Falcon1 Launch Vehicle Payload User Guide," SpaceX 2008.

[21] Cás, P.L.K.D. Vilanova, C.Q. Barcelos Jr, M.N.D. and Veras, C.A.G., "An optimized hybrid rocket motor for the SARA platform reentry system," *Journal of Aerospace Technology and Management*, vol. 4, no. 3, pp. 317-330, 2012, https://doi.org/10.5028/jatm.v4i3.173.

[22]M.M. Fernandez, "Propellant tank pressurization modeling for a hybrid rocket", MSc, Rochester Ins of Technology, Dept. Mech. Eng., Kate Gleason College of Engineering, 2009.

[23] S.S. Chakroborty, M. Wollen, and L. Malany, "Development and optimization of a tridyne pressurization system for pressure fed launch vehicles," In *42nd AIAA/ASME/SAE/ASEE Joint Propulsion Conference & Exhibit*, Sacramento, California, AIAA, Art. No. 4716, 2006, https://doi.org/10.2514/6.2006-4716.

[24] S. Sadullah Khan, M. A. Ahmad, and I. Qamar, "Optimization of pressure-fed liquid propellant rocket engine using various techniques and objectives," *Journal of Space Technology*, vol. 12, no. 1, pp. 39-48, 2022.

[25] G. P. Sutton and O. Biblarz, *Rocket propulsion elements*, 9th edition ed., Wiley, Canada, (2017).

[26] A. S. Pillai, "Introduction to Rocket Science and Space Exploration", *in CRC Press*, Dehradun, India 2023.

[27] D.K. Huzel, and D.H. Huang, "Modern Engineering for Design of Liquid-Propellant Rocket Engines", *in AIAA*, Washington, vol. 147, pp. 135-154, 1992.

[28] Veris, A. d. e., "Fundamental Concept of Liquid-Propellant Rocket engines", *in Springer Aerospace Technology*, Rome, Italy, 2021.

[29] A. Adami, M. Mortazavi, M. Nosratollahi, M. Taheri, and J. Sajadi, "Multidisciplinary design optimization and analysis of hydrazine monopropellant propulsion system," *International Journal of Aerospace Engineering*, Article ID 295636, 9 Pages, 2015, https://doi.org/10.1155/2015/295636.

[30] H. Es-haghnia, "Multidisciplinary design optimization of a two-stage launcher with non-turbopump propulsion system", MSc Thesis, Dept. Aero. Eng., Malek Ashtar Univ., Iran, 2020, (in Persian).

[31] S.L. Kulhanek, "Design, Analysis, and Simulation of Rocket Propulsion System," MSc Thesis, Kansas Univ., Manhattan, 2012.

[32] C.D. Brown, "Spacecraft Propulsion", *AIAA*, Ohio, 1930.

[33] F.A. Silva Mota, "Modeling and Simulation of Launch Vehicles Using Object-Oriented Programming", PhD dissertation, Ins. NDPE, São José, 2015.

[34] R.W. Humble, G.N. Henry, and W.J. Larson, *Space Propulsion Analysis and Design*, New York, San Francisco, Auckland, Bogota: *McGraw-Hill*, 1997.

[35] M. Hosseini, A. Toloie, M. Nosratollahi, and A. Adami, "Multidisciplinary design optimization of an expendable launch vehicle," In *Proceedings of 5th International Conference on Recent Advances in Space Technologies - RAST2011*, Istanbul, Turkey, 2011, 10.1109/RAST.2011.5966932.

[36] L. Brevault, M. Balesdent, and A. Hebbal, "Multi-objective multidisciplinary design optimization approach for partially reusable launch vehicle design," *Journal of Spacecraft and Rockets*, vol. 57, no. 2, pp. 373-390, 2020, https://doi.org/10.2514/1.A34601.

[37] A.J. Masterman, "The Leon 1: A 3D Printed Liquid Methane/ Liquid Oxygen Pressure-fed Rocket Propulsion System", MSc Thesis, Dept. Aero. Eng., San Jose Univ., 2015.

[38] "Environmental Assessment for the operation and Launch of the Falcon 1 and Falcon 9 Space Vehicles," CAPE Canaveral Air Force Station, Florida, Orlando, Florida, 2007.

[39] S. Corbet, "Design of 3rd Stage Rocket for the SPARTAN Space Launch System", Bachelor Thesis, Queensland Univ., 2020.

[40] H. Es-haghnia, N. Nosratollahi, and A. Adami, "Performance evaluation of a launch vehicle with non-turbopump propulsion system based on multidisciplinary analysis (MDA)", *Journal of Space Science and Technology*, vol. 14, no. 4, pp. 35-49, 2021, (in Persian), 10.22034/jsst.2021.1278.

[41] L. Brevault, M. Balesdent, and S. Defoort, "Preliminary study on launch vehicle design: Applications of multidisciplinary design optimization methodologies", *Concurrent Engineering*, vol. 26, no. 1, pp. 93-103, 2018, https://doi.org/10.1177/1063293X17737131

[42] F. Maggi, "Preliminary Design, Modelling, and Comparison of Green and Toxic Rocket Engines For Kick Stages Applications," Politecnico Milano, M.Sc. thesis Engineering, Milan, Italy, 2023.

HOW TO CITE THIS ARTICLE

M. Nosratollahi, H. Es-haghnia, A. H. Adami, "Evaluation of Non-Turbopump Feed Systems for Application in a Two-Stage Launch Vehicle," *Journal of Aerospace Science and Technology*, Vol. 18, Issue 2, 2025, pp. 127-144.

DOI: https://doi.org/10.22034/jast.2025.482120.1211

URL: https://jast.ias.ir/article_235168.html